Article

Inhaled SARS-CoV-2 vaccine for single-dose dry powder aerosol immunization

https://doi.org/10.1038/s41586-023-06809-8

Received: 29 April 2022

Accepted: 31 October 2023

Published online: 13 December 2023

Check for updates

Tong Ye[1,2,13], Zhouguang Jiao[1,13], Xin Li[1,3,13], Zhanlong He[4,13], Yanyan Li[4], Fengmei Yang[4], Xin Zhao[4], Youchun Wang[5], Weijin Huang[5], Meng Qin[6], Yingmei Feng[7], Yefeng Qiu[8], Wenhui Yang[9], Lingfei Hu[9], Yaling Hu[10], Yu Zhai[10], Erqiang Wang[10], Di Yu[11,12], Shuang Wang[1], Hua Yue[1], Yishu Wang[1,2], Hengliang Wang[3]✉, Li Zhu[3]✉, Guanghui Ma[1,2]✉ & Wei Wei[1,2]✉

The COVID-19 pandemic has fostered major advances in vaccination technologies[1–4]; however, there are urgent needs for vaccines that induce mucosal immune responses and for single-dose, non-invasive administration[4–6]. Here we develop an inhalable, single-dose, dry powder aerosol SARS-CoV-2 vaccine that induces potent systemic and mucosal immune responses. The vaccine encapsulates assembled nanoparticles comprising proteinaceous cholera toxin B subunits displaying the SARS-CoV-2 RBD antigen within microcapsules of optimal aerodynamic size, and this unique nano–micro coupled structure supports efficient alveoli delivery, sustained antigen release and antigen-presenting cell uptake, which are favourable features for the induction of immune responses. Moreover, this vaccine induces strong production of IgG and IgA, as well as a local T cell response, collectively conferring effective protection against SARS-CoV-2 in mice, hamsters and nonhuman primates. Finally, we also demonstrate a mosaic iteration of the vaccine that co-displays ancestral and Omicron antigens, extending the breadth of antibody response against co-circulating strains and transmission of the Omicron variant. These findings support the use of this inhaled vaccine as a promising multivalent platform for fighting COVID-19 and other respiratory infectious diseases.

COVID-19, a severe acute respiratory syndrome caused by SARS-CoV-2, was declared a pandemic in 2020[7,8]. Vaccination has been a successful public health intervention for preventing and controlling the spread of this disease[1]. To date, multiple types of SARS-CoV-2 vaccines, such as inactivated vaccines[9,10], protein subunit vaccines[2,11], mRNA vaccines[3,12] and viral-vectored vaccines[4,13], have been approved. Most of these are administered by intramuscular injections that induce the production of serological IgG, thereby neutralizing the infectivity of the virus and alleviating COVID-19. However, vaccines delivered intramuscularly do not provide a first line of protection at the respiratory tract, owing to deficiencies of secretory IgA and IgG[4,5].

Seeking to overcome the problems with intramuscular injection, several vaccine candidates for intranasal or nebulization administration are under development or have been approved[6], most of which are based on viral vectors, such as adenoviruses, attenuated influenza viruses, parainfluenza viruses or Newcastle disease viruses[14–18]. Notably, human clinical studies have shown that inhaled vaccines can induce similar antibody responses to intramuscularly injected vaccines but at a much lower dose than an injected vaccine[19,20]. However, so far, the vaccines developed for intranasal or nebulization administration are in liquid form, necessitating cold chain transportation and storage, and generally require two or three inhaled immunizations or the use of a heterologous booster vaccination.

Given this background and the abundant immune cells known to reside in the lung[21], we were motivated to develop a dry powder vaccine suitable for single-dose inhalation, a goal requiring several considerations. Specifically, the vaccine vector should retain its structure and performance after lyophilization. As smaller particles are liable to be exhaled along with airflow and larger particles tend to deposit in the superficial lung, the aerodynamic size must be well controlled in the 1–4 μm range, enabling predominant deposition in the deep lung[22] (in alveoli). Additionally, vaccine particles with a sustained-release profile can supply continuous antigen stimulation, which may induce a long-lasting immune response.

We initially used the pentameric cholera toxin B subunit (CTB), a potent mucosal adjuvant[23,24], and fused trimer-forming

[1]State Key Laboratory of Biochemical Engineering, Institute of Process Engineering, Chinese Academy of Sciences, Beijing, China. [2]School of Chemical Engineering, University of Chinese Academy of Sciences, Beijing, China. [3]State Key Laboratory of Pathogen and Biosecurity, Beijing Institute of Biotechnology, Beijing, China. [4]Yunnan Key Laboratory of Vaccine Research Development on Severe Infectious Disease, Institute of Medical Biology, Peking Union Medical College, Chinese Academy of Medical Sciences, Kunming, China. [5]Division of HIV/AIDS and Sex-Transmitted Virus Vaccines, Institute for Biological Product Control, National Institutes for Food and Drug Control (NIFDC) and WHO Collaborating Center for Standardization and Evaluation of Biologicals, Beijing, China. [6]Beijing Advanced Innovation Center for Soft Matter Science and Engineering, College of Life Science and Technology, Beijing University of Chemical Technology, Beijing, China. [7]Beijing Youan Hospital, Capital Medical University, Beijing, China. [8]Laboratory Animal Center, Academy of Military Medical Science, Beijing, China. [9]State Key Laboratory of Pathogen and Biosecurity, Beijing Institute of Microbiology and Epidemiology, Beijing, China. [10]Sinovac Life Sciences Co., Ltd., Beijing, China. [11]Frazer Institute, Faculty of Medicine, The University of Queensland, Brisbane, Queensland, Australia. [12]Ian Frazer Centre for Children's Immunotherapy Research, Child Health Research Centre, Faculty of Medicine, The University of Queensland, Brisbane, Queensland, Australia. [13]These authors contributed equally: Tong Ye, Zhouguang Jiao, Xin Li, Zhanlong He. ✉e-mail: wanghl@bmi.ac.cn; jewly54@bmi.ac.cn; ghma@ipe.ac.cn; weiwei@ipe.ac.cn

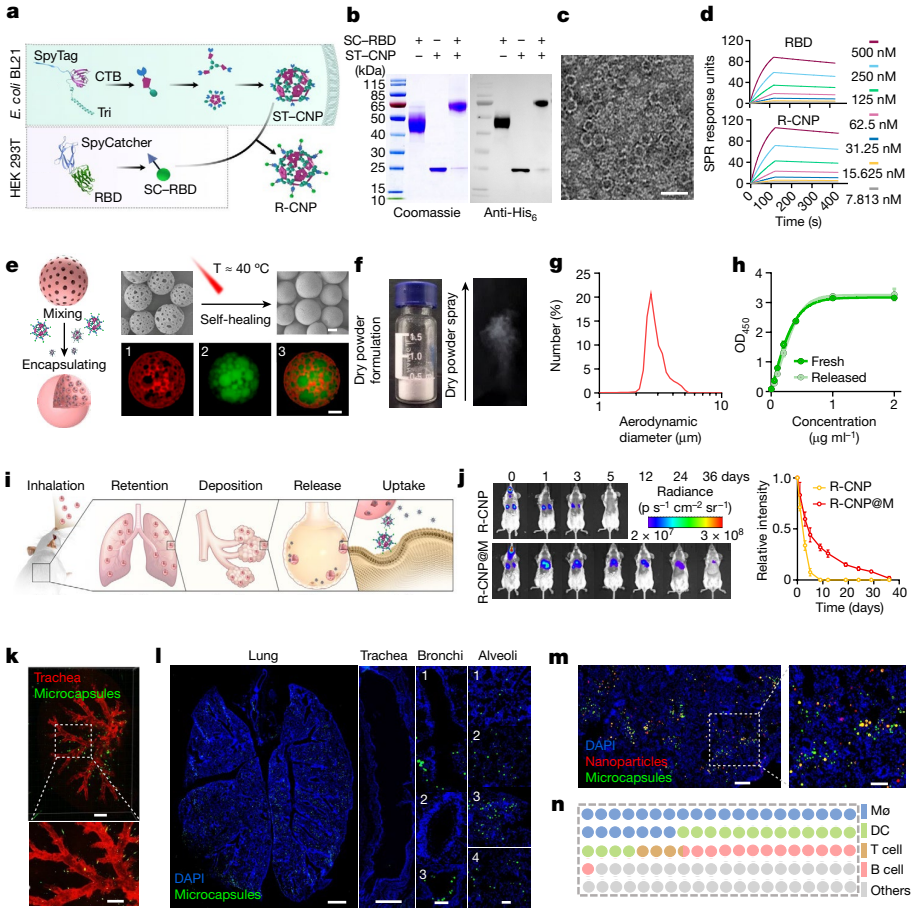

Fig. 1 | Construction of the inhalable R-CNP@M vaccine and pulmonary delivery evaluation in mice. a, Schematic illustration of the preparation of R-CNPs. Tri, trimer-forming peptide. **b**, SDS–PAGE and western blot of covalent complex formation between SC–RBD and ST–CNP. For gel source data, see Supplementary Fig. 1. **c**, Transmission electron microscopy images of R-CNPs. Scale bar, 50 nm. **d**, Surface plasmon resonance (SPR) assay of unconjugated RBD and R-CNPs. **e**, Characteristics of the micro-encapsulation process. The porous microspheres were mixed with R-CNPs to enable penetration (left), which was followed by 40 °C incubation to induce self-healing (right). 1: Red, microcapsule; 2: Green, R-CNP; 3: Merge, R-CNP@M. Scale bars, 2 μm. **f**, Morphology of lyophilized R-CNP@M (left) and corresponding dry powder aerosol (right). **g**, Aerodynamic size of lyophilized R-CNP@M. **h**, Comparison of hACE2 binding affinity between fresh R-CNPs and released R-CNPs. **i**, Schematic illustration of R-CNP@M delivery. R-CNP@M was delivered to the lung and deposited in the alveoli for sustained release of R-CNPs, which was favourable for uptake by APCs. **j**, Representative images of the Cy7-labelled R-CNP signal (left) and corresponding quantitative fluorescence intensity values (right) at the indicated time points. **k**, Light-sheet imaging showing the overall biodistribution of R-CNP@M in the lung. The trachea and bronchi were labelled with streptavidin–AF647 and microcapsules were labelled with Nile red. Scale bars: 500 μm (top), 200 μm (bottom). **l**, Distribution of R-CNP@M in various lung structures. Nuclei and microcapsules were labelled with DAPI and Nile red, respectively. Different numbers represent different areas of the bronchi or alveoli. Scale bars: 1 mm, 500 μm, 100 μm and 100 μm (left to right). **m**, In vivo fluorescence imaging showing that R-CNPs were released from microcapsules on day 10. Cell nuclei were labelled with DAPI. Scale bars: 200 μm (left) and 100 μm (right). **n**, The proportion of different cell types internalizing antigens in the lung (among R-CNP$^+$ cells, assessed by flow cytometry). DC, dendritic cell; Mø, macrophage. Fluorescence images in **k**–**m** are shown in false colour. Data in **h** ($n = 3$ samples) and **j** ($n = 6$ mice) are shown as mean ± s.e.m.

peptides to assemble a self-adjuvanting CTB-based self-assembled nanoparticle (CNP) chassis, which supported the display of SARS-CoV-2 receptor-binding domain (RBD) (R-CNP) based on a bioorthogonal system and enhanced uptake by antigen-presenting cells (APCs) owing to its small size. Next, we encapsulated R-CNPs into porous poly(lactic-co-glycolic acid) (PLGA) microcapsules, and the resulting R-CNP@M, with an optimized aerodynamic diameter, facilitated dry powder aerosol delivery to alveoli. Along with gradual degradation of microcapsules, R-CNPs were released in a sustained manner and were internalized by APCs, leading to potent T cell and B cell responses. Following a single dose, the vaccine induced high IgG and IgA production in mice, hamsters and nonhuman primates, and conferred efficient protection against SARS-CoV-2. Further, an engineered 'mosaic iteration' of this vaccine showed promise for readily responding to future cocirculation of multiple strains and for preventing transmission of the Omicron variant.

Fabrication of R-CNP

Mucosal adjuvanticity and the pentamer domains of CTB initially prompted us to construct a self-adjuvanting nano chassis, which was achieved by the fusion of a trimer-forming peptide at the C terminus of CTB and was subsequently expressed in the *Escherichia coli* BL21 strain[25] (Fig. 1a). Via a SpyTag (ST)–SpyCatcher (SC) bioorthogonal system, the resulting CNP chassis displayed RBD antigens, which are favourable for improving antigen stability, APC uptake and activation[26,27]. As evident from SDS–PAGE and immunoblotting analyses (Fig. 1b and Extended Data Fig. 1a), a clear shift in the molecular weight of the SC–RBD band was observed after mixing with ST–CNP, indicating covalent bond formation. Transmission electron microscopy revealed that the R-CNPs displayed well-dispersed nanoparticulate features (Fig. 1c) and a dynamic light scattering (DLS) analysis showed a narrow size distribution (Extended Data Fig. 1b), with a peak at 24 nm.

Characterization of microcapsules. The filled microcapsules came freeze-dried by freeze dryers (Alpha 2–4 LDplus, Martin Christ Gefriertrocknungsanlagen). The particle sizes of microsphere and microcapsule were analysed by laser diffraction using Mastersizer (Mastersizer 2000, Malvern Instruments). The aerodynamic particle diameter of lyophilized microcapsule was determined by the Aerodynamic Particle Sizer (TSI 3321, TSI). The shape and surface morphology of microsphere, microcapsule, and freeze-dried powder was observed using scanning electron microscopy (JSM-6700, JEOL). To obtain the distribution of nanoparticles in the cavities of the microcapsule, nanoparticles and microcapsules were labelled with FITC–SE and Nile red and observed by using confocal laser scanning microscopy (A1/SIM/STORM, Nikon). Protein concentrations of supernatant after encapsulation were determined by Micro BCA Protein Assay Kit (PI23235, Thermo Scientific) following the corresponding protocols for evaluation of loading capacity (mass of R-CNP in microcapsule/mass of microcapsules × 100%) and encapsulating capacity (mass of R-CNP in microcapsule/mass of total R-CNP × 100%).

In vivo antigen release

To evaluate the duration of nanoparticles with or without microcapsules in vivo, nanoparticle was labelled with near-IR water-soluble fluorescence probe, Cy7–NHS ester (Cy7–SE), and microcapsule was labelled with hydrophobic Cy5 by mixing into the framework during primary emulsion. The inhaled vaccines containing Cy7–nanoparticles and Cy5–microcapsules were delivered into the lung using a customized DPI for mice (Beijing Huironghe Technology). At different time intervals, the mice were captured using a Living Imaging System (Caliper Life Sciences, PerkinElmer), and euthanized to extract organs following capture again at the end of this experiment.

Immunofluorescence analysis

The distribution of R-CNP@M in lung. The animals were vaccinated with Nile Red-labelled R-CNP@M. The lungs were fixed with 4% paraformaldehyde and then dehydrated with 30% sucrose solution for subsequent sectioning on day 5 post-inhalation. Then 10-μm lung slides were prepared by freezing microtome (CM1950, Leica). Slides were mounted for imaging by the Vectra platform (v 3.0.5, PerkinElmer) and counted by inform software.

Germinal centre production of monkey mLNs. The mLNs of the cynomolgus monkeys were collected on day 14 after immunization, the mLNs were fixed with 4% paraformaldehyde and then embedded in paraffin blocks for serial sectioning. Then, 5-μm mLN slides were prepared for immunofluorescence staining. Microwave treatment was conducted with ethylenediaminetetraacetic acid (EDTA) antigen retrieval buffer to retrieve antigen, followed by blocking with 5% (w/v) bovine serum albumin for 30 min. The sections were stained with anti-B220 (F8-11-13, Abcam, ab59168, 1:150), and anti-Ki67 (SolA15, ThermoFisher, 14-5698-82, 1:150) at 4 °C overnight. The corresponding fluorescent secondary antibodies (Abcam, ab150115, 1:10,000; Abcam, ab50168, 1:10,000) were incubated for 1 h at room temperature. Counterstaining was done using DAPI, and slides were mounted for imaging by the Vectra platform.

Light-sheet imaging

To verify whether microcapsules uniformly distribute over the whole lung, lung trachea and microcapsules were labelled with streptavidin–AF647 (Yeasen Biotechnology, 35104ES60, 1:200) and Nile red, respectively. The whole lung was processed with tissue-clearing reagent and captured by light-sheet microscopy (Z.1, Zeiss, Germany). Image reconstructions were generated using Imaris v9.0 software.

To get a visualization of germinal centres in mLNs, B cells were labelled with B220–AF647 (RA3-6B2, Biolegend, 103226, 1:150). The mLNs were profiled by CD31–FITC antibody (W18222B, Biolegend, 160212, 1:150). The mLNs were processed with tissue-clearing reagent and captured in CUBIC-R$^+$ reagent by light-sheet microscopy (Light Innovation Technology). Laser power and gain were adjusted consistently for each group. Image reconstructions were generated using LitScan v3.0 software.

Immunization

Dry powder inhaler. To simulate the process of human dry powder inhalation, we developed a DPI (Supplementary Fig. 2), which comprised the DPAG (Beijing Huironghe Technology), a cushion chamber and an endotracheal tube. To ensure that the dry powder aerosol is inhaled into the lungs through the mouth and trachea, the cushion chamber was designed with one end connected to an endotracheal tube and the other end connected to the DPAG. The volumes of the cushion chamber are distinguished for different animal species (about 35 ml, 80 ml and 700 ml for mouse, hamster, and monkey, respectively). During immunization, the endotracheal tube of DPI is inserted into the animal's trachea, and a needle-free syringe is used as the gas supply source to inject the dry powder vaccine in DPAG into the cushion chamber with the form of dry powder aerosol. The animal is separated from the DPI device after continuously inhaling the dry powder vaccine for 2 min. Note that mouse and hamster can be assisted with a small animal ventilator when using the DPI device.

Immunization for mice. For long-term immunological evaluation, six female BALB/c mice (6–8 weeks old) were immunized twice with R-CNP, which contain 5 μg equivalent SARS-CoV-2 RBD protein intratracheally through a customized liquid aerosol delivery device for mice (Beijing Huironghe Technology); the second dose was the same as the first dose and given on day 14 post-prime vaccination. Six female BALB/c mice (6–8 weeks old) were immunized once with R-CNP@M, which contain 10 μg equivalent SARS-CoV-2 RBD protein intratracheally through DPI for mice. Six female BALB/c mice (6–8 weeks old) were immunized twice with CNP as control.

For the evaluation of mucosal response, another batch of mice was immunized with CNP, R-CNP and R-CNP@M as described above. Six female BALB/c mice (6–8 weeks old) were immunized with 5 μg SARS-CoV-2 RBD protein twice, combined with 100 μg aluminium adjuvant (RBD + Al) through intramuscular route as control, and the second dose was the same as the first dose and given on day 14 post-prime vaccination. On day 70 post-immunization, these mice were euthanized for the collection of BALF and serum. The obtained samples were subsequently inactivated at 56 °C for pseudovirus neutralization assay.

For the live SARS-CoV-2 challenge, another batch of mice was vaccinated with PBS, RBD + Al and R-CNP@M as described above.

Immunization for Syrian golden hamsters. Six-to-seven weeks old female Syrian Golden hamsters were immunized once with R-CNP@M, which contain 30 μg equivalent SARS-CoV-2 RBD protein intratracheally through DPI. Hamsters were intramuscularly immunized three times with licensed recombinant protein subunit vaccine Zifivax, which has been approved for use in China, Colombia, Indonesia and Uzbekistan. The formulation contained 10 μg equivalent of SARS-CoV-2 dimer RBD protein. Blood samples were taken every 14 days, and BALF were collected on the 42nd day. The obtained samples were then subjected to ELISA and live virus neutralization tests. For the live SARS-CoV-2 challenge, another batch of hamsters was vaccinated with PBS, Zifivax and R-CNP@M as described above.

To evaluate the effectiveness of iterative vaccines, six-to-seven weeks old female Syrian Golden hamsters were immunized once with iterative vaccine ($R_{WT}R_O$-CNP@M), which contain 30 μg equivalent SARS-CoV-2 RBD protein intratracheally through DPI. Hamsters were immunized twice with $R_{WT}R_O$ + Al, which contains 15 μg equivalent SARS-CoV-2 RBD protein intramuscularly. Blood samples and BALF were collected on the 42nd day. For the live SARS-CoV-2 challenge, another batch of